Coverage and charge-state dependent adsorption of carbon monoxide on the zinc oxide (0001) surface

M. J. Lyle,[1] O. Warschkow,[1] B. Delley,[2] and C. Stampfl[1]
[1]*School of Physics, The University of Sydney, Sydney, New South Wales 2006, Australia*
[2]*Paul-Scherrer-Institut, Villigen CH-5232, Switzerland*
(Received 23 June 2010; published 1 October 2010)

The adsorption of carbon monoxide (CO) on zinc oxide is important to a number of industrial processes. We report here density-functional calculations of CO binding geometries, adsorption energies, and vibrational frequencies on the polar Zn-terminated ZnO(0001) surface. Our results illuminate a surprising complexity in the adsorbate-surface and adsorbate-adsorbate interactions of this model surface science system, revealing that the nature of the bonding is highly dependent on CO coverage and surface oxidation state.

DOI: 10.1103/PhysRevB.82.165401 PACS number(s): 68.43.Bc, 68.43.Fg, 68.43.Pq, 68.47.Gh

I. INTRODUCTION

Metal oxides are a key component in some of the most widely used heterogeneous catalysts in industry. Zinc oxide (ZnO) plays an important role in the synthesis of methanol,[1] a major technical process with annual production at over 40 million tonnes, representing some U.S. $2 billion per year.[2] Zinc oxide is similarly important as a catalyst in other reactions, such as the hydrogenation of ethylene[3] and the water-gas shift reaction.[4] As a result, the chemical and physical processes that occur on ZnO surfaces, and, in particular, the adsorption of carbon monoxide (CO), have received considerable attention.[5,6]

The adsorption of CO on ZnO has been studied using a wide variety of experimental and theoretical techniques, including temperature programmed desorption,[7–13] near-edge x-ray absorption fine structure measurements,[14–16] x-ray photoelectron spectroscopy,[17,18] helium atom scattering,[19–21] high-resolution electron-energy-loss spectroscopy,[22] and density-functional theory (DFT).[11,23–27] Calculated adsorption energies for CO molecules on the polar Zn-ZnO(0001) surface are reported in the range of −0.19 and −0.54 eV,[24–26] which is in reasonable agreement with recent experimental measurements (−0.28 eV; Ref. 26). The consensus is that CO binds to a single zinc atom in a "top-site" configuration. A recent theoretical study,[28] however, reports that CO at low coverage is more stable in a "bridge-site" configuration between two zinc atoms. This suggests that CO adsorption on this oxide surface is more complicated than previously thought, with an interplay between competing adsorption geometries, not dissimilar to the reported behavior of CO on metal surfaces (see, e.g., Refs. 29 and 30).

In this paper we investigate in detail the coverage and charge-state dependence of CO adsorption on the Zn-ZnO(0001) surface. We survey, for coverages between 1/16 and 1 monolayer (ML), the high symmetry adsorption sites (top, bridge, fcc, and hcp) and examine how the adsorption energies, molecular geometries, and vibrational stretch modes are affected by coverage. The observation of significant charge transfer between surface and molecule leads us to further examine the effects of surface oxidation on these properties. Also observed is that CO molecules, under certain conditions, pair into characteristic dimers and trimers; a phenomenon that we correlate with surface charge transfer. As we will show, the evidently complex behavior of CO on Zn-ZnO(0001) is a direct consequence of surface polarity.

II. COMPUTATIONAL METHODOLOGY

Density-functional theory calculations are performed using the DMOL3 software[31,32] to determine the adsorption energies and structures of CO molecules on the Zn-ZnO(0001) surface. We utilize an atomic orbital basis set of double-numerical quality and additional polarization functions. The basic set is smoothly truncated at 9.25 Bohr for zinc atoms and 9.00 bohr for carbon and oxygen atoms. Exchange correlation is treated in the generalized-gradient approximation using the Perdew, Burke, and Ernzerhof (PBE) functional[33,34] and scalar-relativistic corrections[35] are explicitly incorporated. A thermal broadening of 0.1 eV is applied to the band occupations and our energies are correspondingly reported as Mermin free energies. All calculations are carried out using the spin-restricted formalism of DFT. We have confirmed in trial calculations that spin polarization is not relevant to CO adsorption on Zn-ZnO(0001). These trials were conducted on representative structures for all types of CO bonding configurations (top, bridge, fcc, dimer, trimer; see text below) considered in this work.

The hexagonal bulk unit cell of ZnO is geometry optimized using a $16\times16\times10$ Monkhorst-Pack **k**-point grid.[36] The calculated lattice constants are $a=3.303$ Å and $c=5.315$ Å. The internal lattice parameter is $u=0.3795$. These values are in good agreement with earlier calculations (e.g., Ref. 37; $a=3.282$ Å, $c=5.291$ Å, and $u=0.3792$) and compare well with experimental measurements;[38] between 3.2475 and 3.2501 Å for the a lattice constant and between 5.2042 and 5.2075 Å for c. Experimental values for the internal parameter u are between 0.3817 and 0.3819. Trial calculations using higher mesh densities confirm that total energies and lattice constants of bulk ZnO are converged to well within 0.1 meV/atom and 0.001 Å with respect to **k**-point density.

The ZnO(0001) surface is represented using a three-dimensionally repeated slab model. The slab consists of four double atomic layers of ZnO and is separated from its periodic images by a vacuum slab of approximately 25 Å. Since

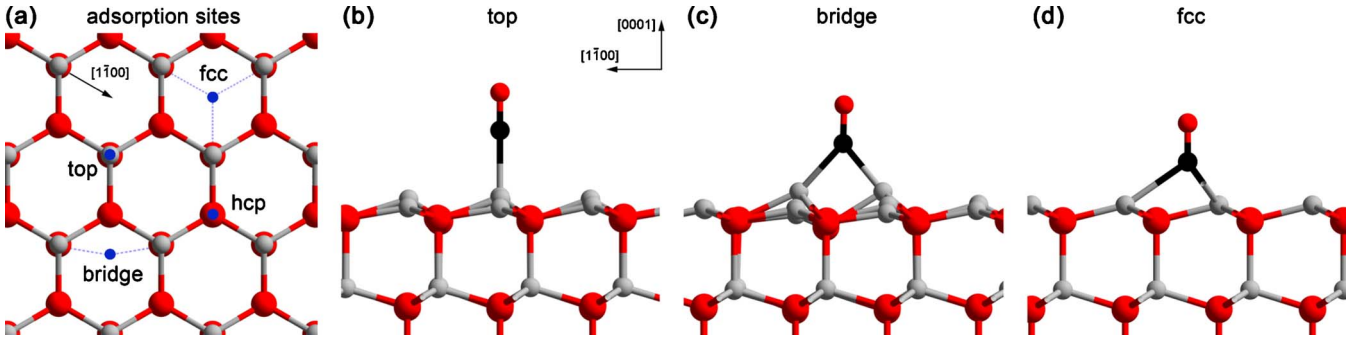

FIG. 1. (Color online) (a) Top view illustration of the four high symmetry adsorption sites—top, bridge, fcc, and hcp—on the Zn-ZnO(0001) surface. Panels (b)–(d) show side views of a CO molecule adsorbed at top, bridge, and fcc sites, respectively. CO does not bind to the surface at the hcp site. Oxygen atoms are represented by dark gray (red) spheres. Zinc and carbon atoms are represented by light gray and black spheres, respectively.

we are considering the Zn-terminated surface in this work, we saturate the O-terminated surface at the bottom of the slab using quasiatoms of nuclear charge $Z=e/2$. As discussed by Meyer *et al.*,[37,39] this ensures that the surface bands of the O-terminated surface are fully occupied so as to quench the residual internal electric field of the polar slab. Full atomic relaxation of the slab is allowed, with the exception of the bottom double atomic layer, and the terminating quasiatoms. The lattice parameters of the slab are held fixed at bulk values. The Brillouin zone of the (1×1) surface slab is sampled using a $(16\times16\times1)$ **k**-point grid with correspondingly smaller grids used for larger supercells.

The CO adsorption energies are calculated as

$$E_{\mathrm{ads}} = E_{\mathrm{slab+CO}} - E_{\mathrm{slab}} - E_{\mathrm{CO}}, \tag{1}$$

where $E_{\mathrm{slab+CO}}$ is the total energy of the adsorbate/substrate system, E_{slab} is the total energy of the clean surface slab, and E_{CO} is the total energy of the gas-phase CO molecule. As defined here, a more negative adsorption energy corresponds to a more stable bonding configuration. We find that a thicker slab model of six ZnO double layers changes the CO adsorption energies by only 0.01 eV. For our purposes, a slab model of four double layers represents a good compromise between energy convergence and computational economy, allowing us to survey adsorption energies and vibrational frequencies for a large number of configurations/unit cell sizes. A dipole correction is applied in our calculations.

Vibrational stretch mode frequencies for CO are calculated via a mass-weighted Hessian matrix that is limited to the atoms of the adsorbates and the topmost ZnO double layer. Trial calculations incorporating further double layers demonstrate that the C-O stretch modes are converged to well below one wave number. The Hessian matrix elements are computed using a three-point finite-difference expression over analytical forces. All optimized geometries are characterized using frequency calculations to distinguish local minima (i.e., stable configurations) from saddle points. We note that saddle point structures are found in our optimizations using high-symmetry structure guesses.

III. RESULTS AND DISCUSSION

A. Adsorption sites in competition

We consider CO adsorption on the Zn-ZnO(0001) surface at the four high-symmetry sites as illustrated in Fig. 1. In the *top* configuration [see Figs. 1(a) and 1(b)], CO is bonded to a single zinc surface atom. In the *bridge* configuration [Figs. 1(a) and 1(c)], the CO molecule bonds to two surface zinc atoms. In the fcc and hcp configurations [Fig. 1(a)], the CO molecule is bonded to three zinc atoms. These latter two sites are distinguished by reference to the oxygen atoms in the second surface layer. The hcp site [Fig. 1(a)] is located above the second layer oxygen atom while the fcc site [Figs. 1(a) and 1(d)] is not. In all configurations, CO is bonded to the surface through the carbon atom. We did not find any stable configurations in which CO is adsorbed through the oxygen atom.

Table I reports our calculated adsorption energies, vibrational modes, and bond lengths for CO adsorption on the ZnO surface. We consider adsorption coverages between 1 ML (i.e., full coverage) and 1/16 ML using $(n\times n)$ unit cells between (1×1) and (4×4), respectively. At full coverage the top configuration is found to be the most stable with an adsorption energy of −0.43 eV, followed by the bridge configuration (−0.23 eV) and the fcc configuration (−0.19 eV). The hcp site is found to be unstable. These findings are consistent with several earlier theoretical investigations.[23–25] For example, Meyer and Marx[24] report an adsorption energy of −0.37 eV for the top configuration at 1 ML, which is in excellent agreement with our result. We have additionally carried out vibrational frequency calculations (at the Γ point) to confirm that the top configuration is a local minimum in a (1×1) unit cell. Similar calculations for the bridge and fcc configurations reveal one and two unstable (imaginary) modes, respectively. This rules out the bridge and fcc configurations as stable minima at full coverage.

Considering CO adsorption at a lower coverage of 1/4 ML, a switch in the preferred adsorption site becomes apparent. At this coverage we find the bridge configuration is the most stable at −0.54 eV. The top and fcc sites are less stable with adsorption energies of −0.48 eV and −0.18 eV, respectively. This switch in preference is due to the considerable

TABLE I. Calculated CO adsorption energies on Zn-ZnO(0001). Vibrational C-O stretch mode frequencies, ν_{CO}, and relevant bond distances (d_{CO} and d_{ZnC}) are also included. Configurations marked with an asterisk have one or more unstable vibrational modes within the unit cell, implying these configurations are saddle points on the potential energy surface. Note that CO in the hcp site does not bind to the surface.

Coverage (ML)	Site	E_{ads} (eV)	ν_{CO} (cm^{-1})	d_{CO} (Å)	d_{ZnC} (Å)
1	Top	−0.43	1994	1.161	2.067
	Bridge*	−0.23	2019	1.162	2.482
	fcc*	−0.19	1957	1.163	2.620
1/4	Top	−0.48	1969	1.162	2.057
	Bridge	−0.54	1778	1.190	2.174
	fcc*	−0.18	1775	1.184	2.484
1/9	Top	−0.51	1917	1.167	2.044
	Bridge	−0.79	1722	1.198	2.114
1/16	Top	−0.57	1908	1.166	2.043
	Bridge	−0.82	1711	1.200	2.141
CO (gas phase)			2124	1.145	

change in the adsorption energy of the bridge configuration; a difference of 0.31 eV between 1/4 and 1 ML. In contrast, the top and fcc energies remain nearly the same (within 0.05 eV). The switch in site preference is also reflected in the vibrational calculations; both bridge and top configurations are now identified as true minima. The fcc configuration has two unstable modes as before.

The trends at 1/4 ML are also found at 1/9 and 1/16 ML. At these two coverages, the bridge configuration is preferred with adsorption energies of −0.79 eV and −0.82 eV, respectively. The top configurations are 0.28 eV and 0.25 eV less stable, respectively.

B. Coverage dependence of CO adsorption

The dependence of the adsorption energies on CO coverage is shown in Fig. 2. In this figure we compare top and bridge sites at ten different coverages between 1/16 and 1 ML, using a variety of unit cells. We note that several of these structures have more than one CO molecule in the unit cell. For example, a 2/3 ML coverage is described using two CO molecules in a $(\sqrt{3}\times\sqrt{3})R30°$ unit cell. There is also a significant effect on the relative arrangement of CO molecules and we explore this using multiple arrangements for a given coverage. Only the most stable structure for a given configuration (top or bridge) is shown in Fig. 2.

The two lines in Fig. 2 connect the lowest energy structures for the top and bridge configurations. Adsorption energies for the top configuration remain relatively constant with respect to coverage with a spread of approximately 0.15 eV over the range. In contrast, the dependence of the bridge configuration on coverage is quite large, changing by approximately 0.6 eV between 1/16 and 1 ML. This leads to a crossover (arrowhead in Fig. 2) in site preference between 1/2 and 2/3 ML: the bridge site is energetically preferred at low coverage while the top site is more stable at high coverage.

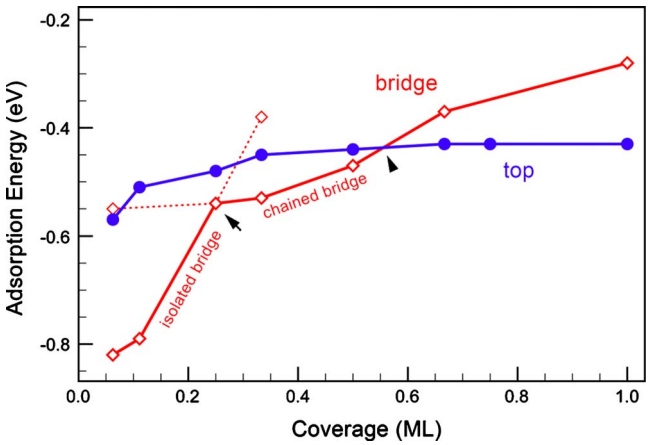

FIG. 2. (Color online) Calculated adsorption energies as a function of CO coverage for the top and bridge sites (blue and red lines, respectively). At approximately 0.55 ML (arrowhead) a switch in preference between top and bridge adsorption sites becomes apparent. At 1/4 ML (arrow), the bridge configuration switches between an isolated and one-dimensionally chained bridge arrangement.

In order to understand these coverage effects, it is instructive to consider the electronic and geometric contributions to the adsorption energy. Table II reports these energy contributions for a CO molecule in a large (4×4) unit cell; our best representation of an isolated adsorbate. The electronic contribution, E_{elec}, is estimated by limiting the geometry optimization to the CO molecule only while keeping all surface atoms fixed at clean surface positions. By subsequently allowing the surface atoms to relax first in the out-of-plane direction (z) and then in the in-plane directions (x,y), we can estimate the respective contributions, $E_{rel,z}$ and $E_{rel,xy}$, to the adsorption energy. This type of analysis shows the bridge configuration to be characterized by much larger relaxation energies than the top configuration. The relaxation energies for the bridge configuration are −0.25 eV and −0.39 eV for in-plane and out-of-plane directions, respectively. This is in contrast to the top configuration where the corresponding energies are much smaller, namely, −0.08 and −0.07 eV. In fact, the adsorption energy in the bridge configuration is largely governed by relaxation effects (both in and out of plane), whereas adsorption in the top configuration is predominantly electronic; without substrate relaxations the top site would be preferred at low coverage.

The effect of coverage on the adsorption energy—large for bridge and small for top—can be understood by inspect-

TABLE II. Adsorption energies for a CO molecule in top and bridge configurations for the (4×4) surface unit cell. The total adsorption energies are decomposed into electronic as well as out-of-plane (z) and in-plane (x,y) relaxation contributions.

Site	E_{ads} (eV)	E_{elec} (eV)	$E_{rel,z}$ (eV)	$E_{rel,xy}$ (eV)
Top	−0.57	−0.42	−0.07	−0.08
Bridge	−0.82	−0.18	−0.39	−0.25

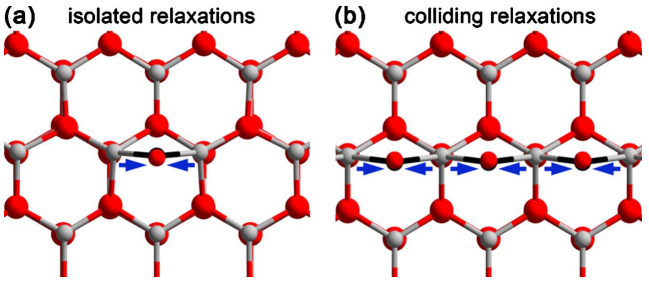

FIG. 3. (Color online) Illustration of in-plane lateral relaxations local to CO molecules adsorbed in the bridge site. (a) An isolated CO induces an inward displacement (arrows) of the two zinc atoms it is bonded to. (b) At higher coverage, these relaxations "cancel" and the zinc atoms remain centered directly above the oxygen atoms. This renders in-plane relaxations less effective as a contribution to the adsorption energy.

ing the atomic relaxations local to the adsorption site. When the density of CO molecules increases, local lateral relaxations begin to "collide" (see Fig. 3) and become less effective in stabilizing the adsorbates. The much larger relaxation energies of the bridge configuration are thus responsible for the more pronounced coverage dependence of the adsorption energy.

At a coverage of 1/4 ML, the bridge configuration undergoes a sharp transition in the energetics (arrow in Fig. 2). Below 1/4 ML, CO molecules prefer to be separated from one another so as to make full use of surface relaxation effects. Above 1/4 ML, there is a preference to form one-dimensional -Zn-CO-Zn-CO-Zn- chains such that surface zinc atoms are bonded to either zero or two CO molecules [see Fig. 3(b)]. In this regime, the dependence of the bridge site adsorption energy on coverage is distinctly reduced. To highlight the transition, we add data points to Fig. 2 for a chained bridge at 1/16 ML and an isolated bridge at 1/3 ML. These points illustrate how the two regimes extend beyond the transition point (indicated by dashed lines).

C. Charge-state dependence of CO adsorption

Looking at the calculated C-O bond lengths in Table I, we observe a consistent shift to larger values for adsorbed CO molecules relative to the gas phase. For example, in the top configuration, the C-O bond distances are between 1.161 and 1.167 Å to be compared with 1.145 Å for the gas-phase molecule. Correspondingly, we find the CO stretch mode frequencies are consistently shifted to lower wave numbers: between 1908 and 1994 cm^{-1} for the top configuration versus 2124 cm^{-1} in the gas phase. Analogous bond length and frequency shifts are found for CO in bridge and fcc sites.

Considering top-site CO at 1/4 ML (see Table III), we find a negative frequency shift, $\Delta\nu_{CO}$, of −155 cm^{-1} (i.e., to smaller wave numbers) and a bond length increase of 0.017 Å, relative to a gas-phase CO molecule. These shifts are consistent with CO acting as an electron acceptor, which is confirmed by Mulliken population analysis (partial charge on the molecule $Q_{CO}=-0.10e$). A density difference plot of this structure [Fig. 4(a)], displays the classical charge transfer pattern in metal-coordinated CO (see, e.g., Refs. 40 and 41): σ-dative bonding is evident midcenter between carbon and zinc as a density accumulation (red) while a significant depletion (blue) around zinc and an enhanced π-shaped density on CO are consistent with zinc backdonation.[42]

TABLE III. Top site CO adsorption on ZnO(0001) surfaces at 1/4 ML using a (2×2) unit cell. We report the adsorption energy, E_{ads}, the C-O stretch mode frequency shift, $\Delta\nu_{CO}$, the C-O bond length shift, Δd_{CO} (both relative to gas-phase CO), and the Mulliken partial charge of the CO molecule, Q_{CO}. In addition to the clean surface, we consider adsorption for two representations of an oxidized surface. One surface is explicitly oxidized by coadsorption of 1/4 ML oxygen atoms ($+O_{fcc}$). A second surface is electronically oxidized by the removal of two electrons from the (2×2) unit cell.

Surface	E_{ads} (eV)	$\Delta\nu_{CO}$ (cm^{-1})	Δd_{CO} (Å)	Q_{CO} (e)
Clean	−0.48	−155	+0.017	−0.10
Oxidized ($+O_{fcc}$)	−0.29	+32	−0.005	+0.08
Oxidized ($-2e$)	−0.44	+55	−0.009	+0.11

The above findings, however, appear to be in conflict with spectroscopic data,[5,43,44] reporting a general shift to larger wave numbers ($\Delta\nu_{CO}\approx+50$ cm^{-1}). On the basis of these results, Solomon *et al.*[5] describe the CO/ZnO active site as one where the molecule acts as an electron donor. It should be noted that the experiments were conducted using ZnO powder samples; thus the probed crystal face and its oxidation state remain unclear. Recent experimental and theoretical work[45,46] provides compelling evidence that the Zn-ZnO(0001) crystal face is in fact oxidized under typical experimental conditions. This raises the possibility that the experimentally reported[5] positive wave number shifts are associated with an oxidized ZnO surface.

In order to test this hypothesis, we calculate CO stretch mode frequencies in the presence of 1/4 ML oxygen adatoms; an *ad hoc* representation of an oxidized surface. On this surface (see Table III) the CO stretch mode is shifted to larger wave numbers ($\Delta\nu_{CO}=+32$ cm^{-1}), in line with the experimental observations,[5] and in contrast with the negative shift calculated for the clean surface. Concomitantly, the C-O bond lengths on the oxidized and clean surface are shortened and lengthened, respectively. Mulliken charges confirm that on the oxidized surface the CO molecule is a weak electron donor ($Q_{CO}=+0.08e$). In place of CO, the oxygen adatom acquires a significant negative partial charge $Q_{O(fcc)}=-0.79e$. The density difference plot for this surface [Fig. 4(b)], reveals a σ-dative bonding pattern similar to that of the clean (nonoxidized) surface, however, the region of significant density depletion is now centered over the CO molecule and zinc backdonation is no longer evident.

The principal effect of the oxygen adatom is to accept electrons according to the nominal equation $\frac{1}{2}O_{2(g)}+2e^{-}\rightarrow O^{2-}_{(ads)}$, lowering the Fermi level of the system. We can imitate this effect for the clean surface in a calculation with two electrons removed from a (2×2) unit cell, taking inspiration from an earlier study[23] which reported positive wave number shifts using a positively charged cluster model. As our data in Table III shows, the calculated

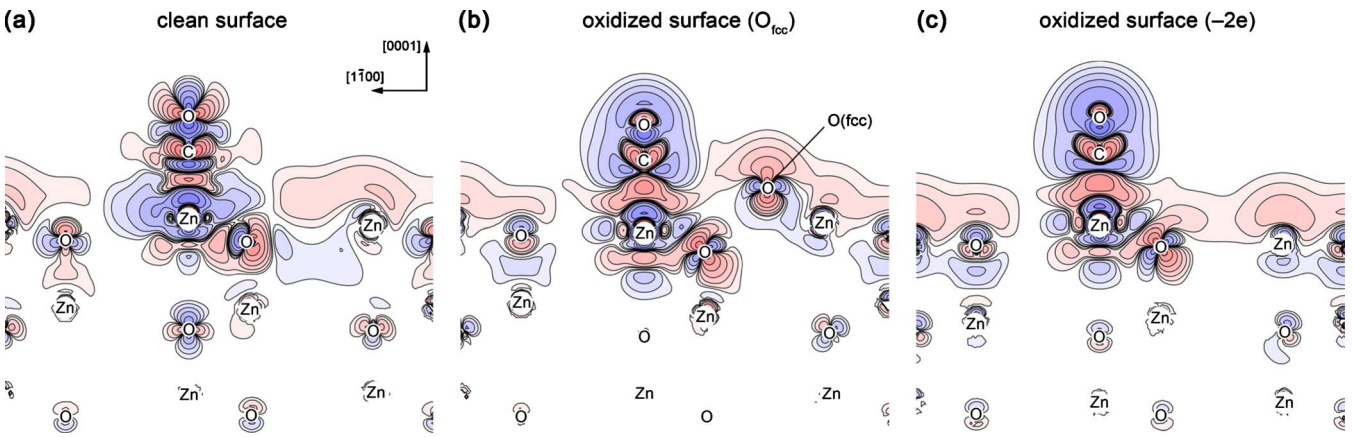

FIG. 4. (Color online) Electron density difference plots ($\rho_{slab+CO}-\rho_{slab}-\rho_{CO}$) for 1/4 ML CO adsorbed on clean and oxidized Zn-ZnO(0001) surfaces. Shown are the cases of CO adsorption (a) on a clean surface, (b) in the presence of O_{fcc} adatom, and (c) on a surface depleted by two electrons per (2×2) unit cell. Charge depletion and accumulation are indicated by blue and red, respectively. Contour lines are ranged between ±0.0001 e bohr^{-3} with successive contours scaled by a factor of $10^{1/3}$. In the case of the electronically oxidized surface, the density difference is calculated using $\rho_{slab+CO}$ and ρ_{slab} both oxidized, while ρ_{CO} remains neutral.

wave number and bond length shifts for the charged surface are positive and negative, respectively, and very close to those of the adatom oxidized surface. Furthermore, the partial charge on the CO molecule ($Q_{CO}=+0.11e$) almost matches the charge found for the explicitly oxidized surface ($Q_{CO}=+0.08e$), and the density difference patterns [Figs. 4(b) and 4(c)] around Zn-CO are nearly identical. This confirms that the CO wave number shifts are associated with the availability of electrons (i.e., the Fermi level) and are not due to strain or steric interactions between the CO molecule and the coadsorbed oxygen.

We note in passing that our geometry optimizations for CO adsorption on the oxygen adatom and electronically oxidized (2×2) surface unit cells did not produce a stable bridge configuration. Thus, the formation of a CO bridge appears to be closely correlated with the surface oxidation state. Moving to a lower oxygen adatom coverage of 1/9 ML, both bridge and top configurations are stable minima, however, the top configuration remains favored (by 0.11 eV). Interestingly, the wave number shift for CO at the top site is negative ($\Delta\nu_{CO}=-118$ cm^{-1}), as on the clean surface, and the molecule is an electron acceptor ($Q_{CO}=-0.06e$). These findings suggest that the surface is no longer sufficiently oxidized for CO to become a donor. At an even lower oxygen coverage of 1/16 ML, the CO adsorption characteristics are effectively those of the clean surface. The bridge site is preferred over top and the wave number shifts are even more negative. Collectively, these results demonstrate that the CO stretch mode frequency is a sensitive probe for the oxidation state of the ZnO surface.

D. Coadsorption effects on surface charge state

The spectroscopic shifts found for top-site CO on an oxidized surface can also be reproduced using coadsorbates other than oxygen. Using the 1/4 ML CO model of the previous section, we consider here the effects of coadsorption with carbon dioxide (CO_2) and hydrogen. One zinc atom in the (2×2) unit cell is occupied by the top CO molecule. The remaining three zinc sites are bonded to either a CO_2 molecule (placed at the hcp site; cf. Ref. 28) or three hydrogen atoms (at top sites).

As shown in Table IV, both carbon dioxide and hydrogen produce positive wave number and negative bond length shifts in the CO molecule, very similar to the shifts found for oxygen adatoms (O_{fcc}). Charge analysis confirms that in all three cases, the coadsorbate acts as an electron acceptor (i.e., $Q_{coads}<0$). Thus, these coadsorbates all act to oxidize the surface, allowing the CO molecule to become an electron donor.

While the three coadsorbates are similar in regards to charge transfer, there is a pronounced difference in their effect on the CO adsorption energy. In comparison to the clean surface ($E_{ads}=-0.48$ eV), the oxygen coadsorbate weakens the CO adsorption energy by 0.19 eV, while CO_2 coadsorption leads to a strengthening by 0.11 eV. Hydrogen coadsorbates have almost no effect on the CO adsorption energy.

A strengthening of the CO adsorption energy by CO_2 coadsorption has been reported by Wang *et al.*[11] on the ZnO$(10\bar{1}0)$ surface. They hypothesize that CO_2 increases the

TABLE IV. Effects of coadsorbates on the binding of CO molecules to the Zn-ZnO(0001) surface. Of the four available zinc sites in a (2×2) unit cell, a top-site CO molecule occupies one zinc atom and the coadsorbate (oxygen, carbon dioxide, or hydrogen) binds to the remaining zinc sites. We report the adsorption energy, E_{ads}, the C-O stretch mode frequency shift, $\Delta\nu_{CO}$, the C-O bond length shift, Δd_{CO}, as well as the Mulliken partial charge of the CO molecule, Q_{CO}, and coadsorbate species, Q_{coads}.

Coadsorbate	E_{ads} (eV)	$\Delta\nu_{CO}$ (cm^{-1})	Δd_{CO} (Å)	Q_{CO} (e)	Q_{coads} (e)
Clean	−0.48	−155	+0.017	−0.10	
O_{fcc}	−0.29	+32	−0.005	+0.08	−0.79
CO_2	−0.59	+65	−0.007	+0.12	−0.77
$3H_{top}$	−0.51	+67	−0.007	+0.11	−0.41

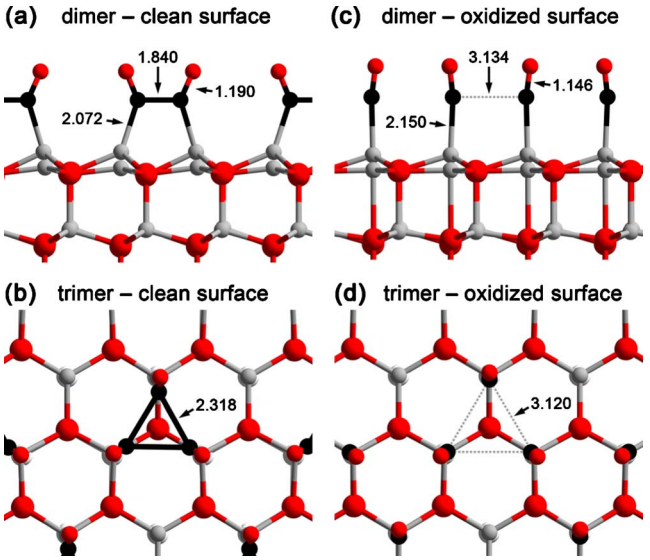

FIG. 5. (Color online) Atomic structures of paired CO structures on the clean and oxidized Zn-ZnO(0001) surfaces. (a) A $(CO)_2$ dimer on the clean surface, calculated at 1/2 ML coverage. (b) A $(CO)_3$ trimer on the clean surface at 3/4 ML. The trimer is centered over an hcp site. [(c) and (d)] On the oxidized surface, CO molecules no longer form dimers and trimers. Selected bond distances (in Å) are indicated.

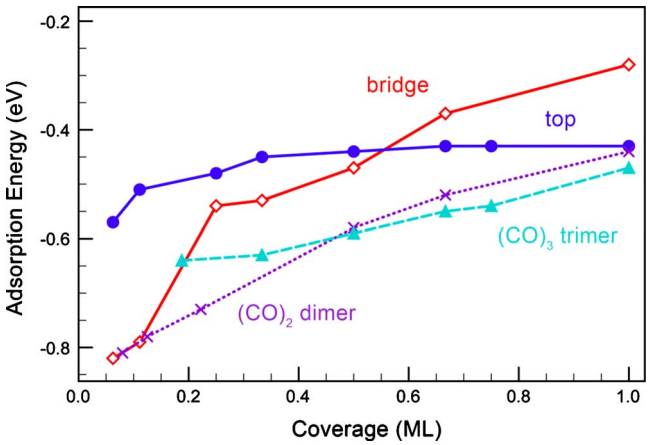

FIG. 6. (Color online) Calculated adsorption energies as a function of coverage for CO molecules in top and bridge configurations. Also included are the adsorption energies of $(CO)_n$ dimer and trimer structures. For the $(CO)_n$ structures, coverage refers to the number of individual CO molecules per unit cell.

Lewis acidity of any vacant zinc sites and propose that coadsorption can be used to tune the reactivity of the surface. Our results for CO_2 coadsorption suggest that a similar mechanism is in effect on the Zn-ZnO(0001) surface. However, the weakening of the CO adsorption energy for oxygen coadsorption, and the absence of any effect for hydrogen coadsorption, indicates that the CO adsorption energy is not solely determined by the charge-accepting properties of the coadsorbate.

E. Pairing of CO adsorbates at high coverage

Related to surface oxidation, we find an interesting pairing phenomenon in our top-site CO structures. Intuitively, CO molecules in a top configuration are expected to adopt a linear Zn-C-O geometry, consistent with a σ-dative bond. In our calculations, however, we find when two or three CO molecules are positioned at nearest zinc sites, they tend to relax toward each other, forming prototype $(CO)_n$ dimer and trimer configurations. This differs sharply from the behavior reported for metal surfaces (e.g., Refs. 30, 47, and 48), where the interaction between CO adsorbates is observed to be repulsive.

On the clean Zn-ZnO(0001) surface, the interaction is attractive, as illustrated in Fig. 5(a), for example, of a dimer formed by two CO molecules in a (2×2) unit cell. In this structure the Zn-C-O geometry is now angled (134°) such that the C-C distance between the two molecules is reduced to 1.840 Å. This distance is considerably shorter than one lattice constant (a=3.303 Å) which would apply for CO molecules in a linear top configuration, though still larger than a typical covalent bond (~1.4 Å). Similarly [see Fig. 5(b)], three CO molecules in a (2×2) unit cell relax into a $(CO)_3$ equilateral trimer with a Zn-C-O bond angle of 139° and a C-C distance of 2.318 Å. A dense packing of $(CO)_3$ trimers with a C-C distance of 2.498 Å occurs for a full monolayer of CO molecules in a $(\sqrt{3}\times\sqrt{3})R30°$ unit cell. We note in passing that $(CO)_3$ trimers occur in two variants, centered over an fcc or hcp site; the hcp-centered trimer is slightly (<0.03 eV per CO molecule) more stable.

Figure 6 shows the coverage-dependent adsorption energies for the $(CO)_n$ dimer and trimer configurations in comparison to the idealized top and bridge structures discussed above. Across the coverage range, we find the paired structures to be more stable than the pure (i.e., unpaired) top configurations. This stabilization is largest at low coverage (>0.2 eV) and decreases almost linearly to become very small (0.04 eV) at a full monolayer. Broadly speaking, we find that the adsorption energies of dimers and trimers are similar ($\Delta E_{ads}<0.15$ eV) at comparable coverages. In detail, $(CO)_3$ trimers are slightly preferred at high coverage while $(CO)_2$ dimers are favored at intermediate coverages. At low coverage (1/9 ML and below), the adsorption energies of the dimers are practically identical to those of the bridge configuration.

Calculated pairing energies, E_{pair}, are reported in Table V for two trimers and one dimer. These pairing energies are defined here as an adsorption energy difference relative to a reference structure in which the CO molecules are constrained to an ideal linear top configuration. Following the overall trends seen in Fig. 6, we find for the 1/2 ML dimer structure a significant pairing energy of −0.14 eV per CO molecule, which is reduced to −0.11 and −0.04 eV for the 3/4 and 1 ML trimer structures, respectively.

The pairing of CO molecules is again intimately linked to the surface oxidation state. As shown in Fig. 5, the removal of two electrons per (2×2) unit cell causes a dimer [Fig. 5(a)] and a trimer structure [Fig. 5(b)] to become distinctly unpaired in Figs. 5(c) and 5(d), respectively. This finding is quantified in Table V, showing that E_{pair} in the oxidized structures becomes very small (<0.02 eV) independent of

TABLE V. Carbon monoxide dimer and trimer structures on clean and oxidized Zn-ZnO(0001) surfaces. The pairing energies, E_{pair}, are calculated relative to the CO molecules adopting an ideal linear top configuration. Also reported are the Zn-C-O bond angles, α_{ZnCO}, and Mulliken partial charges per CO molecule, Q_{CO}.

Coverage (ML)	Surface	E_{ads} (eV)	E_{pair} (eV)	d_{CC} (Å)	α_{ZnCO} (deg)	Q_{CO} (e)
1/2 (dimer)	Clean	−0.58	−0.14	1.840	134	−0.18
	Oxid.	−0.37	−0.01	3.134	170	+0.06
3/4 (trimer)	Clean	−0.54	−0.11	2.318	139	−0.15
	Oxid.	−0.33	−0.02	3.120	163	+0.02
1 (trimer)	Clean	−0.47	−0.04	2.498	146	−0.13
	Oxid.	−0.27	0.00	3.294	178	+0.01

coverage. Likewise, the Zn-C-O bond angles approach that of an ideal linear top configuration (i.e., 180°) and the separation between CO molecules increases to greater than 3 Å. Clearly, the CO molecules are no longer bonded together.

Negative Mulliken partial charges, Q_{CO}, in Table V confirm that CO remains an electron acceptor when in a dimer or trimer configuration on the clean surface. On the oxidized surface, the now unpaired CO molecules are electron donors, as before for isolated CO. We observe in Table V that the pairing energy increases, complemented by a shortening of the C-C separation, as electrons are transferred to $(CO)_n$.

The correlation between charge transfer (Q_{CO}) and $(CO)_n$ geometry is further examined in Fig. 7 for the cases of a symmetric (C_{3v}) trimer and a dimer in a (2×2) surface unit cell. To this unit cell up to four electrons are added and up to three electrons are removed to produce a charge transfer, Q_{CO}, in the range −0.37 to +0.15 e per CO molecule. As shown in Fig. 7, an increasingly negative partial charge results in an almost linear deviation in the C-C separation from

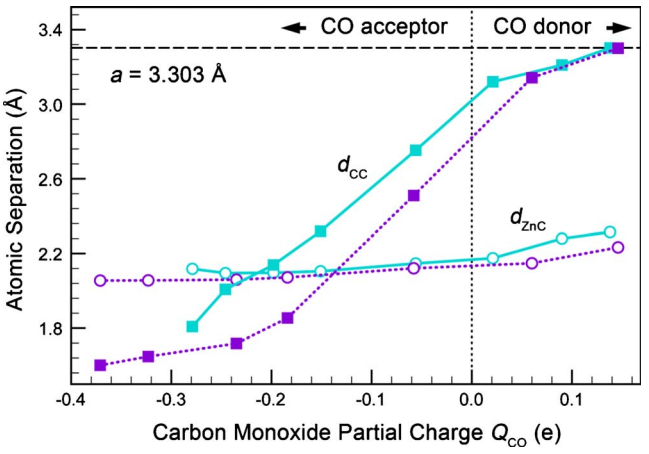

FIG. 7. (Color online) Calculated structural parameters of an adsorbed $(CO)_3$ trimer (solid, cyan line) and $(CO)_2$ dimer (dotted, purple line) as a function of the charge transfer between surface and molecule. Reported are the atomic separations between carbon atoms, d_{CC}, and between carbon and zinc atoms, d_{ZnC}, for $(CO)_n$ in a (2×2) surface unit cell. The charge transfer is quantified by the Mulliken partial charge, Q_{CO}, given in units of e per CO fragment.

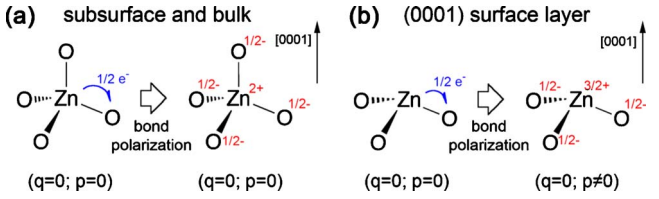

FIG. 8. (Color online) Schematic illustration of the effects of bond polarization in ZnO. (a) Charge transfer for a tetrahedrally coordinated zinc site, leading to a zero net dipole moment (nominally 1/2 electron per Zn-O bond). (b) Charge transfer for a trigonal pyramidal surface zinc atom leads to a finite dipole in the [0001] direction and 1/2 residual electrons on zinc.

an ideal top configuration (horizontal dashed line); saturating in the case of the dimer to approximately 1.6 Å. This confirms that the formation of $(CO)_n$ dimers and trimers is directly related to CO acting as an electron acceptor.

IV. DISCUSSION AND CONCLUSIONS

The preceding sections have highlighted that CO adsorption on Zn-ZnO(0001) is a highly variable process in terms of geometry, energetics, and surface coverage. We have closely examined (see Fig. 6) the close competition between bridge and top configurations over the coverage range with top CO molecules further distinguished into paired (dimer and trimer) and unpaired structures. By considering coadsorption of CO with oxygen atoms (Table III) and surfaces artificially depleted of electrons (Tables III and V), we were able to correlate the favored adsorption geometry with the amount of charge transfer between surface and CO. As we will now discuss, these geometric trends are directly attributable to the polar nature of the Zn-ZnO(0001) surface.

The polarity of Zn-ZnO(0001) can be conceptualized in a variety of ways.[37,46,49,50] For this discussion, it is most convenient to consider surface polarity to be a direct consequence of Zn-O bond polarity. Zinc and oxygen atoms in bulk ZnO are tetrahedrally (i.e., fourfold) coordinated by atoms of the opposite type, as illustrated schematically for zinc in Fig. 8(a). Bond polarization nominally transfers the charge equivalent of 1/2 an electron from the zinc atom to each of its four oxygen neighbors, producing a net charge of +2 on zinc and −1/2 on oxygen (adding to −2 when the contributions from four zinc neighbors are combined). Concomitant with bond polarization, the conduction and valence bands become zinclike and oxygenlike, respectively. Importantly, the bond dipoles in this symmetric tetrahedral arrangement cancel; that is, the local dipole moment, p, is zero. Such a cancellation does not occur for zinc atoms in the (0001) surface plane, which are bonded to three oxygen atoms in a trigonal pyramidal arrangement [Fig. 8(b)]. The absence of a fourth ligand due to crystal truncation means that only 3/2 electrons are transferred to oxygen, leaving 1/2 *residual electrons* on the zinc atom. This is unsatisfactory for two reasons. First, the three bond dipoles no longer cancel, combining to a finite surface dipole moment along the [0001] direction ($p\neq0$). Second, the residual 1/2 electrons on the zinc atom occupy the conduction band which exacts an en-

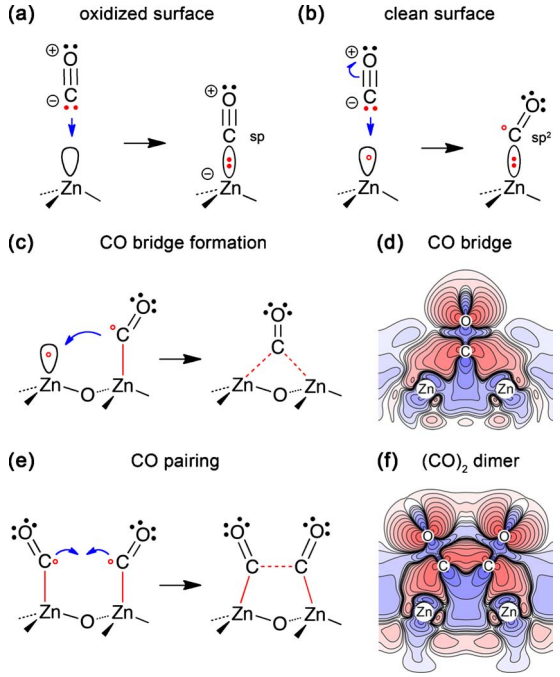

FIG. 9. (Color online) Schematic valence structure diagrams illustrating the mechanism for CO adsorption on the Zn-ZnO(0001) surface. Panels (a) and (b) describe top-site adsorption on the oxidized and clean surface, respectively. For the clean surface, a small open circle is used to represent the residual surface electrons. Panels (c) and (e) describe secondary reactions leading to bridge formation and CO pairing at low and high coverages, respectively. Panels (d) and (f) show the electron density difference $(\rho_{\mathrm{slab}+n\mathrm{CO}}-\rho_{\mathrm{slab}}-n\rho_{\mathrm{CO}})$ for a CO bridge and $(\mathrm{CO})_2$ dimer. Charge depletion and accumulation are indicated by blue and red, respectively. Contour lines are ranged between ± 0.0001 e bohr^{-3} with successive contours scaled by a factor of $10^{1/3}$.

ergy penalty of approximately one band gap per electron. In consequence, there exist strong forces in the Zn-ZnO(0001) surface to shift these electrons into any atoms *above* the surface, and any vacant orbitals created below the conduction band. In the absence of molecular adsorbates, these forces drive the surface to reconstruct into various nonstochiometric forms, including the well-known triangular pits.[45,46] When adsorbate molecules are present, they instead are used to stabilize the surface; the bonding characteristics are determined by the molecule's ability to act as an electron acceptor.

In the case of CO, this leads to a surprising complexity in the substrate-adsorbate interaction. Figure 9 provides a schematic rationalization of the varied geometries CO adopts in response to its local adsorption environment.

It is instructive to first consider the case of top-site adsorption for an oxidized surface [Fig. 9(a)], where the residual surface zinc electrons are absent. The CO molecule binds to the zinc site, providing the two electrons to form a σ-dative bond. In this reaction, the carbon atom remains sp hybridized and the Zn-C-O geometry is linear. This is consistent with our calculations (see Sec. III C): a linear, top-site CO is found to be a global minimum on a (2×2) surface with two electrons per unit cell (or $1/2$ e per surface zinc atom) removed. The same geometry is also found for surfaces that are explicitly oxidized (e.g., by coadsorption with oxygen, carbon dioxide, or hydrogen).

On the clean (nonoxidized) surface, the residual electrons on zinc come into play. As illustrated in Fig. 9(b), CO adsorption again involves σ-dative bond formation between the molecule and zinc. The residual zinc electrons are backdonated into CO, reducing the surface dipole and fractionally populating the π^* orbitals of the molecule. In turn, the molecule responds by tilting (i.e., forming a Zn-C-O angle), which breaks the π^* degeneracy and shifts the residual electrons onto a sp^2-hybridized carbon atom. The formation of bridge-site CO, and paired $(\mathrm{CO})_n$ clusters, is a direct manifestation of the molecule's attempt to stabilize this excess charge.

At low coverage, stabilization is achieved through CO bridge formation, as illustrated in Figs. 9(c) and 9(d). In this case, the residual electron on the CO molecule pairs with the residual electron on a nearby zinc atom to form a second Zn-CO bond. The pairing of fractionally occupied molecular orbitals leads to a net gain in energy that, in turn, drives the bridge formation process. This is consistent with the results in Fig. 2: the bridge site is favored over the top site when the adsorbate coverage is below 1/2 ML (i.e., one CO molecule for every two surface zinc atoms). At higher coverages, an alternative mechanism exists, namely, CO pairing [Figs. 9(e) and 9(f)], in which two or three molecules will share their excess charge to effect a bonding interaction between them; note the distinct density enhancement (red) between the two carbon atoms in Fig. 9(f). Again, fractionally occupied orbitals are combined and energy is gained.

The role of the residual electrons in these secondary bond formation processes is confirmed by our calculations on oxidized Zn-ZnO(0001). Oxidation, as discussed above, removes these electrons from the surface and secondary bond formation is no longer required as a stabilization mechanism. This is evidenced by the absence of stable bridge structures (see Sec. III C) or CO pairing (see Fig. 5). Top-site CO is the preferred configuration on the oxidized surface.

From the perspective of catalysis, it is instructive to consider Zn-ZnO(0001) surface oxidation as a coadsorption phenomenon; oxygen adatoms, and other oxidizing species (e.g., zinc vacancies), are simply regarded as another type of adsorbate species in competition with the reactants (e.g., CO). This viewpoint is motivated by the fact that all four adsorbate species considered here (CO, oxygen, CO_2, and hydrogen) are found to be electron acceptors when placed on the clean surface. The transfer of electrons into any adsorbate is driven by the polarity of the Zn-ZnO(0001) surface which, as discussed above, exerts strong forces to promote its residual electrons into the above-surface plane. In the case of coadsorption, i.e., more than one type of adsorbate on the surface, there will be competition over which adsorbate will accept these electrons. This is presumably determined by the relative electron affinity of the coadsorbates. In keeping with this, we find that CO, as a highly reluctant electron acceptor, is a donor in the case of coadsorption. The bonding characteristics of CO are thus highly dependent on what other species are bound to the surface.

In summary, calculations of CO adsorption on the

Zn-ZnO(0001) surface demonstrate that numerous bonding configurations can arise as a function of adsorbate coverage and surface oxidation state in the presence of coadsorbing species. The polarity of the Zn-ZnO(0001) surface, specifically the role of residual electrons, is critical to understanding the CO adsorption properties.

ACKNOWLEDGMENTS

We gratefully acknowledge the financial support of the Australian Research Council under Discovery Grant No. DP0770631. Computational resources are provided by the National Computation Infrastructure (NCI).

[1] G. Ertl, H. Knözinger, and J. Weitkamp, *Handbook of Heterogeneous Catalysis* (VCH, Weinheim, 1997).
[2] "Methanex" Annual Information Form, 2009; Management's Discussion and Analysis, 2009, http://www.sedar.com
[3] R. J. Kokes, Acc. Chem. Res. **6**, 226 (1973).
[4] D. S. Newsome, Catal. Rev. - Sci. Eng. **21**, 275 (1980).
[5] E. I. Solomon, P. M. Jones, and J. A. May, Chem. Rev. **93**, 2623 (1993).
[6] Ch. Wöll, Prog. Surf. Sci. **82**, 55 (2007).
[7] S. Akhter, K. Lui, and H. H. Kung, J. Phys. Chem. **89**, 1958 (1985).
[8] W. H. Cheng and H. H. Kung, Surf. Sci. **122**, 21 (1982).
[9] M. Bowker, H. Houghton, K. C. Waugh, T. Giddings, and M. Green, J. Catal. **84**, 252 (1983).
[10] D. L. Roberts and G. L. Griffin, J. Catal. **110**, 117 (1988).
[11] Y. Wang, X. Xia, A. Urban, H. Qiu, J. Strunk, B. Meyer, M. Muhler, and Ch. Wöll, Angew. Chem., Int. Ed. **46**, 7315 (2007).
[12] X. Xia, J. Strunk, R. Naumann d'Alnoncourt, W. Busser, L. Khodeir, and M. Muhler, J. Phys. Chem. C **112**, 10931 (2008).
[13] X. Xia, R. Naumann d'Alnoncourt, and M. Muhler, J. Therm Anal. Calorim. **91**, 167 (2008).
[14] A. Gutiérrez-Sosa, S. Crook, S. Haq, R. Lindsay, A. Ludviksson, S. Parker, C. T. Campbell, and G. Thornton, Faraday Discuss. **105**, 355 (1996).
[15] R. Lindsay, A. Gutiérrez-Sosa, G. Thornton, A. Ludviksson, S. Parker, and C. T. Campbell, Surf. Sci. **439**, 131 (1999).
[16] A. Gutiérrez-Sosa, T. M. Evans, S. C. Parker, C. T. Campbell, and G. Thornton, Surf. Sci. **497**, 239 (2002).
[17] C. T. Au, W. Hirsch, and W. Hirschwald, Surf. Sci. **197**, 391 (1988).
[18] R. Lindsay, E. Michelangeli, B. G. Daniels, T. V. Ashworth, A. J. Limb, G. Thornton, A. Gutiérrez-Sosa, A. Baraldi, R. Larciprete, and S. Lizzit, J. Am. Chem. Soc. **124**, 7117 (2002).
[19] Th. Becker, Ch. Boas, U. Burghaus, and Ch. Wöll, Phys. Rev. B **61**, 4538 (2000).
[20] Th. Becker, M. Kunat, Ch. Boas, U. Burghaus, and Ch. Wöll, J. Chem. Phys. **113**, 6334 (2000).
[21] M. Kunat, B. Meyer, F. Traeger, and Ch. Wöll, Phys. Chem. Chem. Phys. **8**, 1499 (2006).
[22] Y. Wang, B. Meyer, X. Yin, M. Kunat, D. Langenberg, F. Traeger, A. Birkner, and Ch. Wöll, Phys. Rev. Lett. **95**, 266104 (2005).
[23] M. Casarin, E. Tondello, and A. Vittadini, Surf. Sci. **303**, 125 (1994).
[24] B. Meyer and D. Marx, J. Phys.: Condens. Matter **15**, L89 (2003).
[25] S. Shou-heng, S. Chuan, K. Fink, and V. Staemmler, Chem. Phys. **287**, 183 (2003).
[26] V. Staemmler, K. Fink, B. Meyer, D. Marx, M. Kunat, S. G. Girol, U. Burghaus, and Ch. Wöll, Phys. Rev. Lett. **90**, 106102 (2003).
[27] P. M. Jones, J. A. May, J. B. Reitz, and E. I. Solomon, Inorg. Chem. **43**, 3349 (2004).
[28] K. Chuasiripattana, O. Warschkow, B. Delley, and C. Stampfl, Surf. Sci. **604**, 1742 (2010).
[29] J. G. Love, S. Haq, and D. A. King, J. Chem. Phys. **97**, 8789 (1992).
[30] S. J. Jenkins and D. A. King, Surf. Sci. **504**, 138 (2002).
[31] B. Delley, J. Chem. Phys. **92**, 508 (1990).
[32] B. Delley, J. Chem. Phys. **113**, 7756 (2000).
[33] J. P. Perdew, K. Burke, and M. Ernzerhof, Phys. Rev. Lett. **77**, 3865 (1996).
[34] J. P. Perdew, K. Burke, and M. Ernzerhof, Phys. Rev. Lett. **78**, 1396 (1997).
[35] B. Delley, Int. J. Quantum Chem. **69**, 423 (1998).
[36] H. J. Monkhorst and J. D. Pack, Phys. Rev. B **13**, 5188 (1976).
[37] B. Meyer and D. Marx, Phys. Rev. B **67**, 035403 (2003).
[38] Ü. Özgür, Y. I. Alivov, C. Liu, A. Teke, M. A. Reshchikov, S. Doğan, V. Avrutin, S.-J. Cho, and H. Morkoç, J. Appl. Phys. **98**, 041301 (2005).
[39] B. Meyer and D. Marx, Phys. Rev. B **69**, 235420 (2004).
[40] P. Hu, D. A. King, M.-H. Lee, and M. C. Payne, Chem. Phys. Lett. **246**, 73 (1995).
[41] M. Gajdoš, A. Eichler, and J. Hafner, J. Phys.: Condens. Matter **16**, 1141 (2004).
[42] Electrons backdonated from zinc occupy the π^* molecular orbital of CO. In the density difference plot [Fig. 4(a)], these electrons are responsible for the two-lobed density enhancement (red) around the carbon and oxygen atoms.
[43] D. A. Seanor and C. H. Amberg, J. Chem. Phys. **42**, 2967 (1965).
[44] R. Gay, M. Nodine, V. Henrich, H. Zeiger, and E. Solomon, J. Am. Chem. Soc. **102**, 6752 (1980).
[45] O. Dulub, U. Diebold, and G. Kresse, Phys. Rev. Lett. **90**, 016102 (2003).
[46] G. Kresse, O. Dulub, and U. Diebold, Phys. Rev. B **68**, 245409 (2003).
[47] P. Hu, D. A. King, S. Crampin, M.-H. Lee, and M. C. Payne, J. Chem. Phys. **107**, 8103 (1997).
[48] H. Kato, M. Kawai, and J. Yoshinobu, Phys. Rev. Lett. **82**, 1899 (1999).
[49] P. W. Tasker, J. Phys. C **12**, 4977 (1979).
[50] C. Noguera, J. Phys.: Condens. Matter **12**, R367 (2000).